Effect of a base cavity on the wake modes of the squareback Ahmed body at various ground clearances and application to drag reduction.

G. BONNAVION[a], O. CADOT[a], V. HERBERT[b], S. PARPAIS[c], R. VIGNERON[d], J. DÉLERY[d]

a. IMSIA, ENSTA-ParisTech, UMR 9219 CNRS, 828 Boulevard des Maréchaux, 91762 Palaiseau Cedex, France; bonnavion@ensta.fr
b. Groupe PSA, Route de Gisy, 78140 Vélizy-Villacoublay, France
c. Renault Technocentre Guyancourt, 1 avenue du Golf, 78288 Guyancourt Cedex, France
d. GIE S2A, 2 Avenue Volta, 78180 Montigny-le-Bretonneux, France

Résumé :

Récemment, une réduction de traînée de l'ordre de 9% *a été obtenue sur un corps non profilé, le corps d'Ahmed à culot droit, une géométrie simplifiée de véhicule terrestre, grâce à l'utilisation d'une cavité au culot [2]. Les auteurs associent cette réduction à la suppression des modes statiques asymétriques du sillage identifiés dans [4], permettant ainsi la symétrisation de celui-ci. L'effet bénéfique d'une cavité de culot sur la traînée est connu depuis des décennies pour des corps non profilés axisymétriques dans le contexte de l'ingénierie aéronautique [6] mais le phénomène n'a pas encore été complètement élucidé à ce jour. Notre travail vise à montrer expérimentalement que la réduction de l'asymétrie du sillage proche est associée à la diminution de la traînée quelle que soit la garde au sol. Pour ceci, nous effectuons deux études paramétriques en garde au sol d'un corps d'Ahmed à culot droit dans une soufflerie industrielle : sans et avec une cavité au culot. Suffisamment loin du sol, c'est-à-dire après la bifurcation pour l'arrière-corps sans cavité, les modes statiques asymétriques disparaissent comme indiqué dans [2] : l'écoulement est symétrisé et la pression de culot augmente de* 24%*. De plus, à proximité du sol, deux nouveaux résultats sont présentés dans ce papier. Les modes du sillage ne sont pas les mêmes qu'à grande garde au sol mais sont plutôt verticaux en raison de la proximité du sol. De plus, l'asymétrie du sillage est réduite mais pas supprimée par la cavité. Cependant, une réduction de traînée du même ordre de grandeur qu'en régime lointain est observée (*7% *associée à une augmentation de pression au culot de* 20%*).*

Abstract :

Recently, drag reduction by almost 9% *was achieved by means of a base cavity on a three-dimensional bluff body, the squareback Ahmed body, a simplified road vehicle geometry [2]. The authors associate that with the suppression of the static asymmetric modes of the wake identified in [4] leading to its symmetrization. The beneficial effect of a base cavity on drag has been known for decades on axisymmetric bluff bodies in the context of aerospace engineering [6] but the phenomenon has not been fully elucidated yet. The present work aims at showing experimentally that the decrease of the asymmetry of the*

near wake flow is associated with drag reduction regardless of the ground clearance of a squareback Ahmed body. With this aim in mind, we do two parametric studies of the ground clearance of the model in an industrial wind-tunnel; one without and one with a base cavity. Far enough from the ground, i.e. *after the bifurcation for the squareback geometry, the static asymmetric modes of the wake disappear in agreement with [2]; the flow is symmetrized and the base pressure increases by* 24%*. In the vicinity of the ground however, two new results are reported in this paper. The modes governing the wake are not the same as at higher ground clearances but are rather vertical modes due to the presence of the ground. Besides, the wake asymmetry is reduced but not totally suppressed in the near ground regime. Nevertheless, an important drag reduction of the same order of magnitude as in the far ground regime is observed (*7% *associated with a base pressure increase by* 20%*).*

Mots clefs : Contrôle d'écoulement, corps d'Ahmed à culot droit, écoulement décollé, modes à brisure de symétrie, sillage

1 Introduction

Growing issues on energy consumption motivate research activities to identify accurate drag reduction mechanisms for real ground transportation vehicles that would be compatible with a series production. Since the seeding work of Ahmed *et al.* [1], the squareback Ahmed body is commonly studied as a simplified road vehicle geometry. From the academic point of view, it is a bluff body experiencing a full flow separation at its vertical rear part, called the base. This leads to the formation of a recirculating area in which the norm of the velocity is very small with respect to the free-stream flow. Its wake is known to experience a super-critical bifurcation in the laminar regime ($\mathrm{Re} \approx 340$) at which its symmetry is lost [3]. The asymmetry persists when increasing the Reynolds number up to few millions and is associated with the static asymmetric modes of the wake possibly leading to wake bi-stability, *i.e.* random exploration of the modes depending on the model's aspect ratio [4, 5]. Another super-critical bifurcation from a symmetry-preserving state to asymmetric modes operated by the ground clearance of the model was identified with a $1/4^{th}$-scale Ahmed body in the turbulent regime in [5]. Two regimes are identified as a function of the distance away from the ground. Similarly to experiments made with an axisymmetric cylinder [6], passive flow control by means of a base cavity was recently introduced in view of drag reduction with interesting results in the bifurcated state with the asymmetric modes as stable solutions of the wake [2]. The authors associate the improvement with the removal of the static asymmetric modes of the wake but no parameter but the cavity depth is studied in their work. In particular, the effect of the above mentioned bifurcation is not carried out. The present experimental work presents a new description of the bifurcation of the wake operated by the ground clearance and aims at generalizing and explaining the effect of a base cavity before and after the bifurcation. The objective is to obtain a comprehensive analysis that could be used during the development of real road vehicles. The paper is organized as follows. The experimental setup is described in section 2. The results are presented and discussed in section 3 before some concluding remarks are made in section 4.

2 Experimental setup

The model used in this work is a three-dimensional bluff body representing a simplified road vehicle geometry approximately at the $1/5^{th}$-scale, the squareback Ahmed body. It is the same as the one used

in [2] but with an adjustable distance to the ground, called the ground clearance c; its dimensions are reported in Tab. 1 and the body is depicted in Fig. 1*(a-b-c)* with its characteristic dimensions.

Dimension	
Height of the body:	$H = 0.298$ m
Width of the body:	$W = 0.350$ m
Length of the body:	$L = 0.994$ m
Wheelbase:	$WB = 0.477$ m
Projected surface area:	$S = 0.104$ m^2
Aspect ratio:	$W^* = W/H = 1.174$

Table 1: Dimensions of the squareback Ahmed body used in this study.

The model's ground clearance can be adjusted from $c^* = c/H = 0.06$ up to 0.17, owing to two Standa 8MVT188-20 translation stages and their 8SMC4-USB controller. Both axis are imposed to be at the same distance c away from the ground so that the model does not experience any pitch angle ($\alpha = 0°$). It is kept aligned with the incoming flow (yawing angle $\beta = 0°$) throughout.

The base of the body is equipped with a sliding board of dimensions $(W - 20\text{ mm}) \times (H - 20\text{ mm})$ described more precisely in [2] used to create a base cavity. Two configurations only are used in this paper: absence of cavity ($d = 0$), referred as the squareback configuration, and a cavity with a depth $d^* = d/H = 0.285$.

The following coordinate system is used in this paper. The $\vec{e_x}$ axis is aligned with the flow, positive downstream; the $\vec{e_z}$ axis is ground-normal, positive upwards and the $\vec{e_y}$ axis is chosen accordingly to obtain a right-handed coordinate system whose origin is at the bottom of the base, mid track. The coordinate system is related to the body. As a consequence, its origin is always at a distance c away from the ground and is moving with the body.

Throughout this paper, all non-dimensionalizations of any quantity $a(y, z, t)$ are denoted by means of the superscript *. They are performed using the model's height H and the free-stream velocity U_∞. The convective time-scale is consequently $t^* = \frac{t \times U_\infty}{H}$. Upper case letters are used to denote the temporal mean, $A(y, z) = \overline{a}(y, z)$, and the probability density function PDF(a) is used to characterize the behavior of the parameters of study. An averaging over 0.5 s, which corresponds to a dimensionless frequency of $f^* \approx 0.03$, is performed on the data $a(y, z, t)$ as a low-pass filter.

The wall pressure distribution is measured simultaneously at 21 pressure taps located at the base of the body (Fig. 1*b*). The sampling frequency is set to $f = 200$ Hz ($f^* \approx 3$). The measurement is made owing to a Scanivalve ZOC22b pressure scanner connected to a GLE/SmartZOC100 electronics, acquiring the pressure measurement on all channels simultaneously. Its accuracy is of the order of ± 3.75 Pa per channel. The pressure coefficient c_p is defined as follows where p_∞ is the free-stream static pressure obtained directly from the facility:

$$c_p(y^*, z^*, t^*) = \frac{p(y^*, z^*, t^*) - p_\infty}{\frac{1}{2}\rho U_\infty^2}. \tag{1}$$

A global quantity representative of the average pressure level at the base is defined in Eq. (2), the base suction coefficient c_b. The minus sign ensures that c_b has the same evolution as the total drag coefficient c_x defined in this section. The ordered pair (y_i^*, z_i^*) stands for the location (made dimensionless

using H) of the i^{th} pressure sensor ($i = 1, \ldots, 21$).

$$c_b(t^*) = -\frac{1}{21}\sum_{i=1}^{21} c_p(y_i^*, z_i^*, t^*), \tag{2}$$

The base pressure distribution $c_p(y_i^*, z_i^*, t^*)$ is associated with a dimensionless complex base pressure gradient $\hat{G} = \partial_{y^*} c_p(t^*) + \mathrm{i}\, \partial_{z^*} c_p(t^*)$ where $\partial_{y^*} c_p(t^*)$ is the horizontal base pressure gradient and $\partial_{z^*} c_p(t^*)$ the vertical base pressure gradient. The modulus $|\hat{G}|$ and the azimuthal phase $\arg\left(\hat{G}\right)$ (expressed in radians and in $]-\pi, \pi]$) of the complex base pressure gradient $\hat{G}$ are considered hereafter. The computation of the horizontal and the vertical base pressure gradients is detailed below. The instantaneous pressure coefficients are obtained at the points $A,\ B,\ C$ and D in Fig. 1*(b)*. Once the differential pressure is computed, the dimensionless distance between points is used to get the vertical base pressure gradient $\partial_{y^*} c_p(t^*)$:

$$\partial_{y^*} c_p(t^*) = \frac{1}{2} \times \left(\frac{c_p(y_A^*, z_A^*, t^*) - c_p(y_B^*, z_B^*, t^*)}{y_A^* - y_B^*} + \frac{c_p(y_C^*, z_C^*, t^*) - c_p(y_D^*, z_D^*, t^*)}{y_C^* - y_D^*} \right) \tag{3}$$

where $I = A,\ B,\ C,\ D$ and y_I^* and z_I^* stand for the coordinate of point I in the reference system defined above. The same method is applied to compute the vertical base pressure gradient $\partial_{z^*} c_p(t^*)$ using the pairs (A, C) and (B, D).

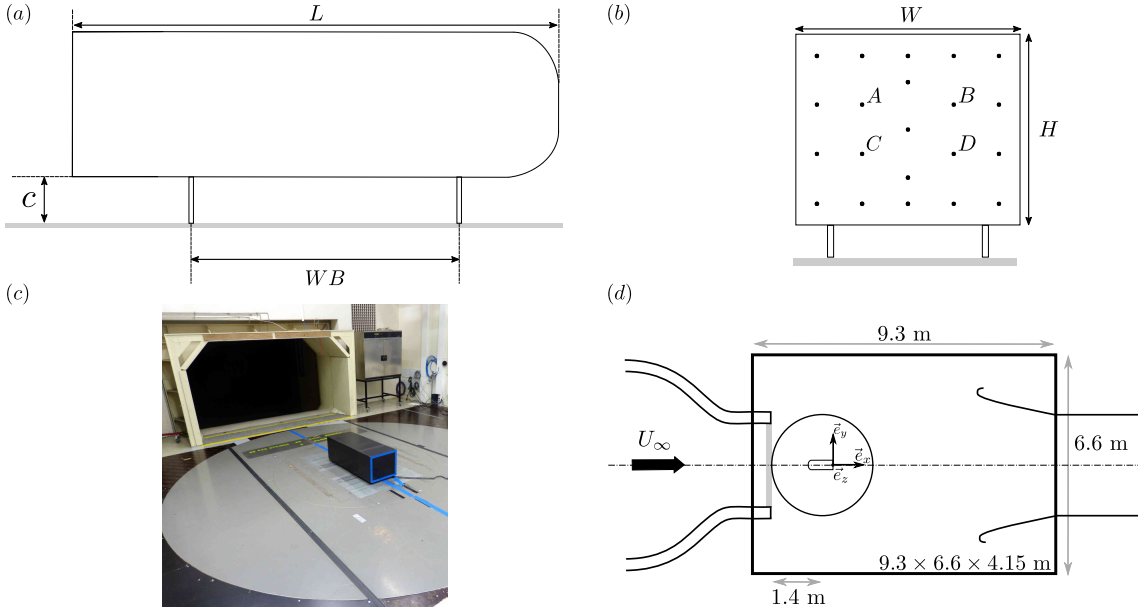

Figure 1: (a) Schematic view of the squareback Ahmed body used in this work and definition of the ground clearance c - (b) Characteristic dimensions of the cross-section $W \times H$ of the body and location of the 21 pressure taps at the base. The points $A,\ B,\ C$ and D are used to compute the base pressure gradients as described in Eq. (3) - (c) Ahmed body in the wind-tunnel GIE-S2A wind tunnel - (d) Schematic view of the test section of the wind tunnel, location of the model and coordinate system.

The drag force f_x is measured with a precision of ± 0.3 N owing to a six-components aerodynamic balance located beneath the wind-tunnel floor to which the four cylindrical supports of the model are connected. Time series are obtained at a sampling frequency of 5 Hz. The drag f_x is non-dimensionalized

into the coefficient of drag c_x:

$$c_x = \frac{f_x}{\frac{1}{2}\rho S U_\infty^2} \tag{4}$$

where ρ is the air density and S the projected model frontal area ($S = 0.104$ m^2).

The inhomogeneity of the pressure distribution is characterized by the spatial standard deviation σ_{c_p}:

$$\sigma_{c_p}(t^*) = \left(< c_p(y^*, z^*, t^*)^2 >_{\text{base}} - c_b(t^*)^2 \right)^{1/2} \tag{5}$$

where $< \cdot >_{\text{base}}$ denotes spatial averaging over the base. Its temporal mean is $\overline{\sigma}_{c_p}$.

The experiments are carried out in the model-scale wind-tunnel of the GIE-S2A at Montigny-le-Bretonneux (France), a schematic of which is given in Fig. 1*(d)*. All tests are performed at a free-stream velocity of $U_\infty = 20$ m.s^{-1} corresponding to a Reynolds number based on the model height of $\text{Re}_H = 3 \times 10^5$. The incoming flow is a $3/4$ open jet with a cross section of 3.84 m^2. At the considered free-stream velocity, the turbulence intensity of the wind-tunnel is less than 0.4%. More details about the facility can be found in [2].

3 Results and discussion

The results are presented as follows. First, we study the effects of the ground clearance on the fluid force, on the base pressure distribution and on the wake in section 3.1. Afterwards, the drag reduction mechanism is investigated in section 3.2.

3.1 Bifurcations of the wake operated by the ground clearance

For the first set of tests, we reproduce the same experiment as in [5] in the range $c^* = 0.06$ up to $c^* = 0.17$. The Probability Density Functions (PDF) of the modulus $|\hat{G}|$ and of the argument $\arg(\hat{G})$ of the complex base pressure gradient $\hat{G}$ are plotted in Fig. 2 with respect to the ground clearance c^*. The PDFs are normalized by their maximum value.

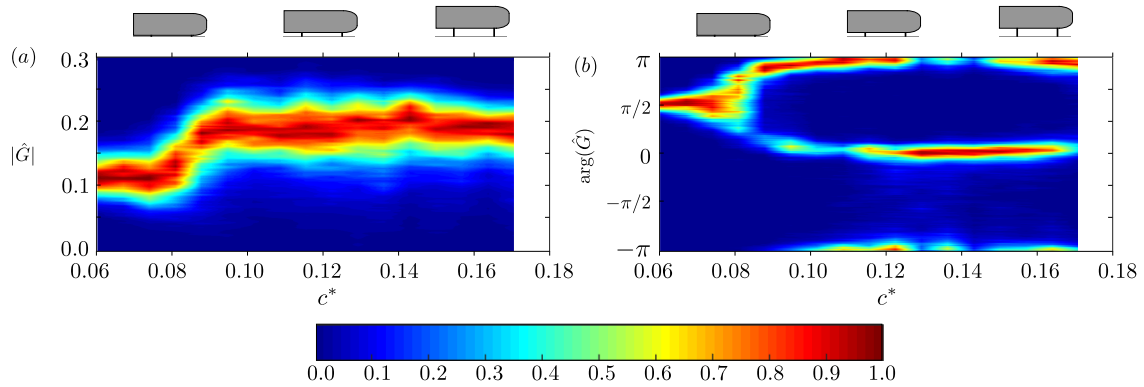

Figure 2: Probability Density Function normalized by the maximum value and plotted against the ground clearance c^* in the squareback configuration ($d^* = 0$): (a) modulus of the base pressure gradient $|\hat{G}|$ - (b) azimuthal phase of the base pressure gradient $\arg(\hat{G})$ (in radians in $]-\pi, \pi]$).

Two different regions can be identified. For $c^* \leq 0.08$, the modulus of the complex base pressure gradient is almost constant with very small fluctuations: $|\hat{G}| \approx 0.12$. In this region, the phase is locked to $\arg\left(\hat{G}\right) = \pi/2$, also with very small fluctuations. The mean base pressure distribution $C_p(y^*, z^*)$

given in Fig. 3 (for $c^* = 0.06$) is permanently selected as proved by the single peak in the PDF's of the base pressure gradients. The wake is symmetric in the horizontal direction. However, in spite of the symmetry of the body, the vertical base pressure distribution is not symmetric due to the close proximity of the ground; the pressure levels are indeed lower at the bottom of the base than at its top thus generating a vertical base pressure gradient.

For $c^* \geq 0.10$, the modulus of the complex base pressure gradient is also constant but has increased with respect to the previous case: $|\hat{G}| \approx 0.18$. Unlike in the previous region, not only one but two preferred values of the phase $\arg\left(\hat{G}\right)$ can be identified: $0\ [2\pi]$ and $\pi\ [2\pi]$, which corresponds to two skew symmetric mirror configurations of the wake. For $0.10 \leq c^* \leq 0.13$, the transitions occur more frequently via the upper part of the base (corresponding to phases in $[0, \pi]$), whereas for $c^* \geq 0.130$ the phases in $[-\pi, \pi]$, corresponding to the bottom part of the base, are more frequently explored. The mirror mean base pressure distributions $C_p(y^*, z^*)$ and the PDFs for base pressure gradients associated with such ground clearances are given in Fig. 4 (for $c^* = 0.12$). The switch between those follows a stochastic behavior [7].

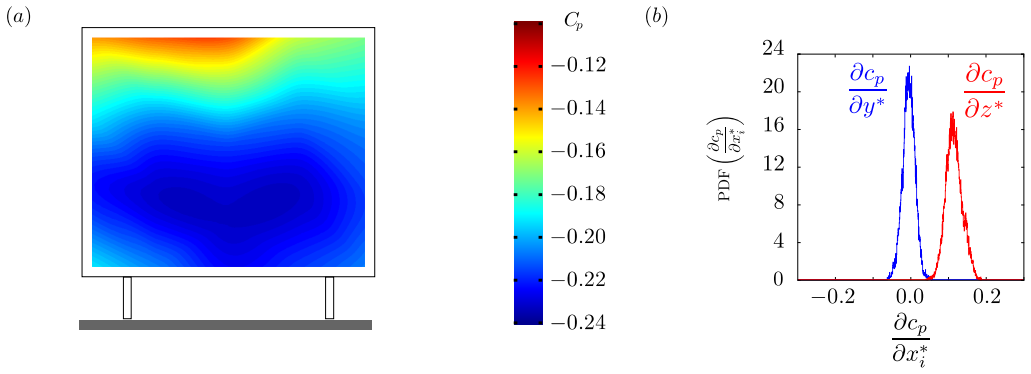

Figure 3: squareback Ahmed body at $c^* = 0.06$: (a) Mean base pressure distribution $C_p(y^*, z^*)$ corresponding to $\arg\left(\hat{G}\right) = \pi/2$ - (b) Associated Probability Density Functions for the vertical (in red) and the horizontal (in blue) base pressure gradients.

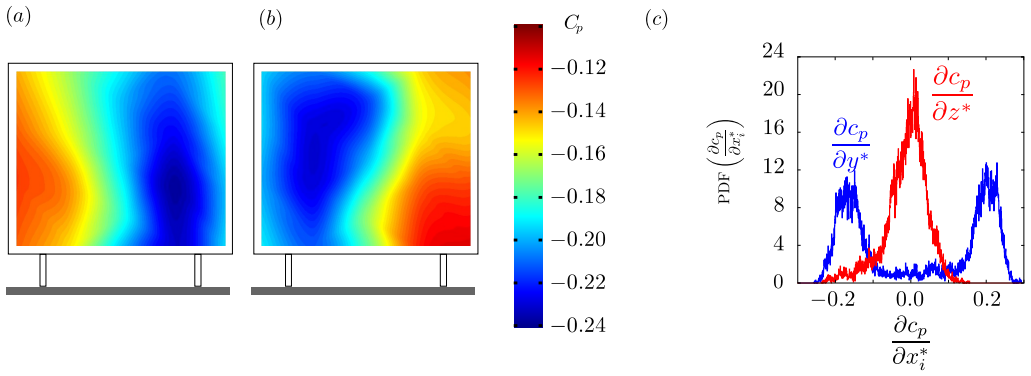

Figure 4: squareback Ahmed body at $c^* = 0.12$: (a) Mean base pressure distribution $C_p(y^*, z^*)$ for $\arg\left(\hat{G}\right) = 0$ - (b) Mean base pressure distribution $C_p(y^*, z^*)$ for $\arg\left(\hat{G}\right) = \pi$ - (c) Probability Density Functions for the vertical (in red) and the horizontal (in blue) base pressure gradients.

In the range $0.08 \leq c^* \leq 0.10$, a very sudden change of behavior can be observed for the modulus which increases continuously with the ground clearance c^* from $|\hat{G}| \approx 0.12$ to $|\hat{G}| \approx 0.18$. This

change is associated with a phase unlocking; the fluctuations grow linearly in the range $[-\pi, \pi]$ until wake bi-stability described before is reached for $c^* = 0.10$. This threshold corresponds consequently to a bifurcation of the wake operated by the ground clearance. These results presented above are in total agreement with those of [5] and can possibly be extended to scales similar to those of real road vehicles.

For the second set of experiments, we create a base cavity at the body (depth $d^* = d/H = 0.285$). The PDFs in the $(|\hat{G}|, \arg(\hat{G}))$ variables are given in Fig. 5 as a function of the ground clearance c^*. The

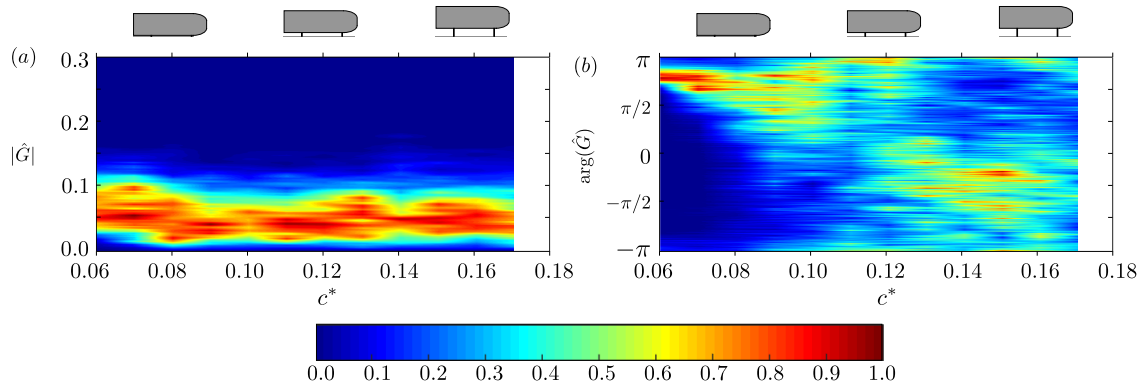

Figure 5: Probability Density Function normalized by the maximum value and plotted against the ground clearance c^* with the base cavity ($d^* = 0.285$): (a) modulus of the base pressure gradient $|\hat{G}|$ - (b) azimuthal phase of the base pressure gradient $\arg(\hat{G})$ (in radians in $]-\pi, \pi]$).

modulus of the gradient is significantly attenuated on the whole range of ground clearances considered here and is now almost constant for all the points considered: $|\hat{G}| \approx 0.06$, which represents a reduction by respectively 50% and 65% with respect to the near ground and far ground configurations. As for the phase, two regions can still be observed. For $c^* \leq 0.075$, it remains locked at $\arg\left(\hat{G}\right) = \pi/2$ with small fluctuations only. The associated mean base pressure distribution $C_p(y^*, z^*)$ is given in Fig. 6. The scale is the same as for the squareback shape and clearly denotes a base pressure recovery. The vertical base pressure gradient can still be observed though. For higher ground clearances, all angles in $[-\pi, \pi]$ have almost the same probability. As the modulus of the gradient is very small, this proves that the wake is symmetrized, as shown in the associated mean base pressure distribution $C_p(y^*, z^*)$ (Fig. 6).

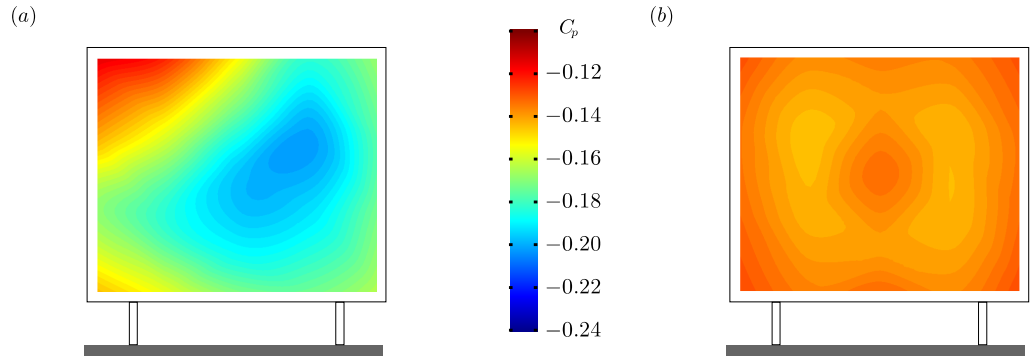

Figure 6: squareback Ahmed body with a base cavity ($d^* = 0.285$) - Mean base pressure distribution $C_p(y^*, z^*)$: (a) For $c^* = 0.06$ - (b) For $c^* = 0.12$

The results of [2] can consequently be generalized for $c^* \geq 0.075$. Below this threshold, the phase-

locking phenomenon at $\arg(\hat{G}) = \pi/2$ observed before is conserved for the complex base pressure gradient. Phase-unlocking occurs above. These two new regions will then be compared with the unbifurcated and the bifurcated regions identified before in terms of base drag. In a previous work [2], drag reduction by nearly 9% was obtained. The authors associate this gain with the removal of the static asymmetric modes of the wake. In this paper, we suggest a plausible explanation for the drag reduction mechanism.

3.2 Mechanism for drag reduction

Drag is plotted as a function of the ground clearance for the squareback geometry and with the base cavity, together with the relative gain with control in Fig. 7. It can be observed that the beneficial effect of the base cavity is present regardless of the ground clearance. Above the threshold $c^* = 0.08$, compared to the squareback geometry, drag reduction by 8% is achieved, almost regardless of the ground clearance. As in [2], the mean flow is symmetrized (Fig. 6). The mean base suction coefficient C_b decreases by 23.5% in average, which explains the reduction of the total drag. The same behavior is expected below the threshold as the wake bifurcation is believed to be operated by a static asymmetric mode as well. At $c^* = 0.06$, base pressure increases by 15% which leads to 4.8% drag reduction. However, the flow is not fully symmetrized as a remaining phase (at $\arg(\hat{G}) = \pi/2$) can be identified for the complex base pressure gradient (Fig. 6). With respect to the far ground regime, drag reduction loses efficiency. The close proximity to the ground influences the flow around the body and has a detrimental effect on drag.

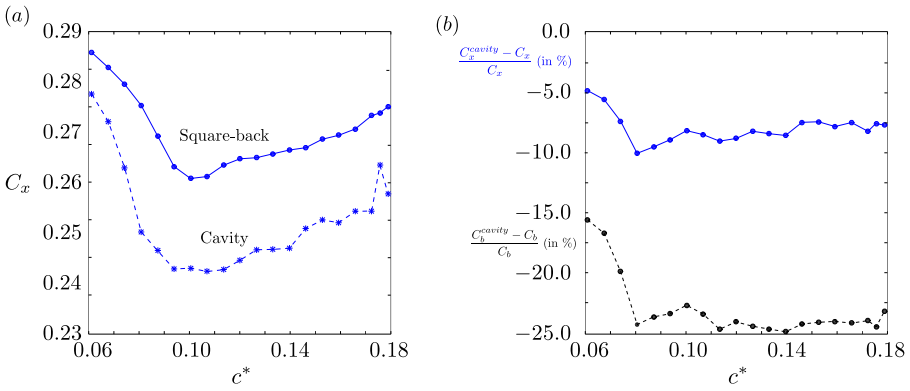

Figure 7: (a) Mean drag coefficient C_x of the Ahmed body plotted as a function of the ground clearance c^* for the squareback (solid line) and the base cavity (dashed line) geometries. - (b) Relative reduction for the controlled case plotted as a function of the ground clearance c^*: mean base suction C_b (black dashed line), mean drag C_x (blue continuous line).

The mean spatial standard deviation of the wake $\overline{\sigma}_{c_p}$ defined in Eq. (5) is considered to investigate whether the wake inhomogeneity can be related to drag. In Fig. 8, the mean base suction coefficient C_b is plotted as a function of $\bar{\sigma}_{c_p}$ for the cases without and with base cavity. It turns out that two groups of points can be identified: those with high drag and high inhomogeneity of the wake, corresponding to the squareback geometry and those with lower inhomogeneity and lower drag associated with the base cavity. The inhomogeneity of the wake is spatially coherent and corresponds to its asymmetry. In short, the larger the asymmetry of the wake, the bigger the drag. The asymmetry of the wake is reduced by the base cavity. This enhances its efficiency as it is not the only mechanism implied.

In addition to the removal of the modes, the geometrical modifications introduced by the cavity indeed have a beneficial effect on drag. In fact, the dead water area (recirculating bubble) is elongated. From

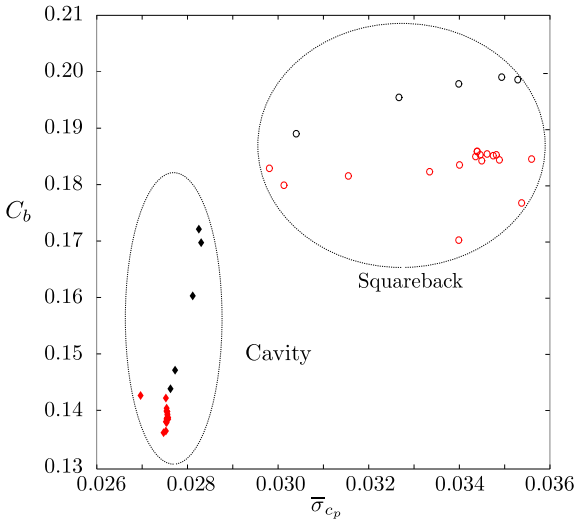

Figure 8: Mean spatial standard deviation of the wake of the Ahmed body $\overline{\sigma}_{c_p}$ plotted as a function of the ground clearance c^* for the squareback (empty circles) and the base cavity (filled diamond shape). Black points are below the threshold at $c^* = 0.080$, red points above.

PIV measurements presented in [2], the reattachment point in the mean flow slightly moves downstream in presence of a base cavity. In addition to that, an additional volume $\mathscr{V}^* = d^* \times (H^* - 0.067) \times (W^* - 0.067)$ is generated as the cavity is created. From [2], the streamlines enter the cavity and are therefore elongated in the upstream direction as well. Since H^* and W^* are imposed, the other characteristic dimensions of the recirculating bubble are unchanged. As a consequence, the inner streamlines' curvature is reduced. It follows that pressure increases at the base of the model. The base suction is thus lowered as well as the total drag.

4 Conclusion

The bifurcation of the turbulent wake of the squareback Ahmed body operated by the ground clearance is described using a polar description. A central rotation of the wake can be observed and phase locking and unlocking phenomenon are responsible for the change of the wake topology. The effect of a base cavity is generalized to both regimes with a minimal gain of about 5% on drag. The base cavity symmetrizes the flow and therefore reduces the asymmetry-related drag but also elongates the recirculating area at the base of the model which allows for pressure recovery. This passive flow control device is already used on trucks and could be optimized to achieve a most efficient drag reduction.

References

[1] S.R. Ahmed, G. Ramm Some Salient Features of the Time-Averaged Ground Vehicle Wake, SAE-Paper, 840300 (1984).

[2] A. Évrard, O. Cadot, V. Herbert, D. Ricot, R. Vigneron, J. Délery Fluid force and symmetry breaking modes of a 3d bluff body with a base cavity, Journal of Fluids and Structures, 61 (2016) 99–114.

[3] M. Grandemange, O. Cadot, M. Gohlke, Reflectional symmetry breaking of the separated flow over three-dimensional bluff bodies, Physical Review E, 86 (2012) 035302-1 – 035302-4.

[4] M. Grandemange, O. Cadot, M. Gohlke, Turbulent wake past a three-dimensional bluff body. Part. 1. Global modes and bi-stability, Journal of Fluid Mechanics, 722 (2013) 51–84.

[5] M. Grandemange, O. Cadot, M. Gohlke, Bi-stability in the turbulent wake past parallelepiped bodies with various aspect ratio and wall effect, Physics of Fluids, 25 (2013) 95–103.

[6] T. Morel, Effect of base cavities on the aerodynamic drag of an axisymmetric cylinder, Aeronautical Quarterly, 30 (1979) 400-412.

[7] G. Rigas, A.S. Morgans, R.D. Brackston, J.F. Morrison, Diffusive dynamics and stochastic models of turbulent axisymmetric wakes, Journal of Fluid Mechanics, 778 (2015) R2.